Novel quantum spin liquid states in the S=1/2 three-dimensional compound Y3Cu2Sb3O14

Saikat Nandi, Rounak Das, Mamoun Hemmida, M. U. Akbar, Hans-Albrecht Krug von Nidda, Jörg Sichelschmidt, Sagar Mahapatra, Marlis Schuller, Norbert Büttgen, J. M. Wilkinson, M. P. Saravanan, Indra Dasgupta, A. V. Mahajan

Angaben zur Veröffentlichung / Publication details:

Nandi, Saikat, Rounak Das, Mamoun Hemmida, M. U. Akbar, Hans-Albrecht Krug von Nidda, Jörg Sichelschmidt, Sagar Mahapatra, et al. 2026. “Novel quantum spin liquid states in the S=1/2 three-dimensional compound Y3Cu2Sb3O14.” *Physical Review Letters* 136 (16): 166502. https://doi.org/10.1103/2bps-xvl8.

Novel Quantum Spin Liquid States in the $S = \frac{1}{2}$ Three-Dimensional Compound $Y_3Cu_2Sb_3O_{14}$

Saikat Nandi,[1,*] Rounak Das,[2] M. Hemmida,[3] M. U. Akbar,[3] H.-A. Krug von Nidda,[3] Jörg Sichelschmidt,[4] Sagar Mahapatra,[5] Marlis Schuller,[3] N. Büttgen,[3] J. M. Wilkinson,[6] M. P. Saravanan,[7] Indra Dasgupta,[2] and A. V. Mahajan[1,†]

[1]*Department of Physics, Indian Institute of Technology Bombay, Mumbai 400076, India*
[2]*School of Physical Sciences, Indian Association for the Cultivation of Science, 2A and 2B Raja S.C. Mullick Road, Jadavpur, Kolkata 700 032, India*
[3]*Experimental Physics V, Center for Electronic Correlations and Magnetism, University of Augsburg, D-86135 Augsburg, Germany*
[4]*Max Planck Institute for Chemical Physics of Solids, 01187 Dresden, Germany*
[5]*Department of Physics, Indian Institute of Science Education and Research, Pune, Maharashtra 411008, India*
[6]*ISIS Pulsed Neutron and Muon Source, STFC Rutherford Appleton Laboratory, Harwell Campus, Didcot, Oxfordshire OX110QX, United Kingdom*
[7]*Low Temperature Laboratory, UGC-DAE Consortium for Scientific Research, Indore, 452001, India*

(Received 21 July 2025; revised 5 March 2026; accepted 26 March 2026; published 22 April 2026)

The three-dimensional $S = \frac{1}{2}$ system $Y_3Cu_2Sb_3O_{14}$ consists of two inequivalent Cu^{2+} sites, each forming an edge shared triangular lattice. Our magnetic susceptibility $\chi(T)$, specific heat $C_p(T)$, ^{89}Y nuclear magnetic resonance (NMR), muon spin relaxation (μSR), and electron spin resonance (ESR) measurements on this system confirm the absence of any long-range magnetic ordering and the persistence of spin dynamics down to 0.077 K. In ^{89}Y NMR, we find an anomaly at about 120 K, which we suggest arises from a fraction of the spins condensing into a singlet (a valence bond solid, or VBS) state. A plateau in the muon relaxation rate is observed between 60 K and 10 K (signifying the VBS state from a fraction of the spins) followed by an increase and another plateau below about 1 K (presumably signifying the quantum spin liquid state from all the spins). Our density functional theory calculations find a dominant antiferromagnetic interaction along the body diagonal with inequivalent Cu(1) and Cu(2) ions alternately occupying the corners of the cube. All other near-neighbor interactions between the Cu ions are also found to be antiferromagnetic and are thought to drive the frustration.

DOI: 10.1103/2bps-xvl8

Introduction—Quantum spin liquids (QSLs) are an exciting playground in many fields of physics, chemistry, theory of quantum computation, and materials science and engineering for exotic physical phenomena and emergent many-body quantum states. The starting point has often been spin-$\frac{1}{2}$ systems with geometric frustration. This approach has led to the discovery of many systems such as the kagome material $ZnCu_3(OH)_6Cl_2$ (or herbertsmithite), triangular-lattice organic compounds κ-$(ET)_2Cu_2(CN)_3$ and $EtMe_3Sb[Pd(dmit)_2]_2$, and vesignieite, $BaCu_3V_2O_8(OH)_2$, which show intriguing signs of QSL behavior [1–3].

A variant of the above is a triangular lattice system, $LiZn_2Mo_3O_8$, where, with decreasing temperature, the triangular magnetic lattice is found to decouple into a combination of free spins and a honeycomb lattice, which then condenses into a valence bond solid (VBS) state [4–6].

While most studies focus on quasi-two-dimensional systems, there has been some work on three-dimensional systems such as those with corner shared tetrahedra, hyperhoneycomb systems. Three-dimensional (3D) arrangements of spin systems exhibit mostly ordered behavior in the absence of a special geometry. A QSL state in an $S = \frac{1}{2}$ system with a 3D geometry and strong frustration has been realized in $PbCuTe_2O_6$ [7].

Our attention has been captured by the rhombohedral pyrochlore family $(RE)_3M_2Sb_3O_{14}$ (RE = Y, La, Pr, Nd, Sm, Eu, Gd, Tb, Dy, Ho, Er, Yb, Lu). This series of materials has a rare-earth (RE) 2D kagome lattice separated by triangular planes of M^{2+} ions [8–21]. However, the cubic phase is preferred with the decreasing size of the lanthanide ion, and the compound $Y_3Mn_2Sb_3O_{14}$ has a cubic pyrochlore structure (space group $Fd\bar{3}m$) [11]. In the past few years, many exotic states have been reported for $(RE)_3Mg_2Sb_3O_{14}$ (RE = Nd, Gd, Dy, Er), such as scalar chiral spin order, dipolar spin order, kagome spin ice, and Kosterlitz-Thouless transition [8]. We have, on the other hand, focused on having a nonmagnetic ion at the rare-earth

*Contact author: saikatnandi9@gmail.com
†Contact author: mahajan@phy.iitb.ac.in

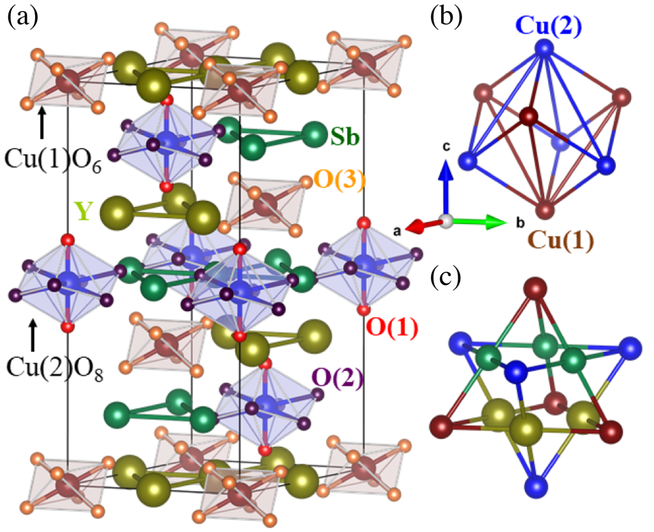

FIG. 1. (a) Crystal structure of $Y_3Cu_2Sb_3O_{14}$ in one unit cell consisting of $Cu(1)O_6$ octahedra and $Cu(2)O_8$ hexagonal bipyramids. The atoms are shown in different colors. (b) Arrangement of the magnetic Cu^{2+} forming 3D frustrated linkages. (c) Cu(1)-Y and Cu(2)-Sb layers composed of Cu(1) and Cu(2) networks.

site while keeping a magnetic ion (Cu^{2+} $S = \frac{1}{2}$) on the M site; i.e., $Y_3Cu_2Sb_3O_{14}$. The aim is to investigate for any novel states due to the triangular Cu^{2+} lattice.

In this Letter, we report a comprehensive study of $Y_3Cu_2Sb_3O_{14}$ through bulk and local probe measurements. While the absence of long-range order down to 0.077 K is evident, our ^{89}Y nuclear magnetic resonance (NMR) data point to a fraction of the spins condensing into a VBS state below about 120 K followed by all the spins going into a gapless QSL state below about 1 K. A similar result is obtained from electron spin resonance (ESR) experiments, where a part of the ESR signal intensity follows the Bleaney-Bowers dimer variation with temperature, with a broad maximum around 120 K [see Supplemental Material (SM) [22] for details]. Muon spin relaxation measurements infer a muon depolarization rate (λ_{ZF}) that increases with decreasing temperature and has plateaus below about 60 K and again below 1 K. The plateau at the higher temperature might signify a decoupling of the frustrated lattice into two components: (i) an emergent lattice with fewer nearest neighbors for each lattice point, which condenses into a VBS state, and (ii) additional free spins. At the lower plateau in the muon relaxation rate, all the spins condense into a gapless QSL state. We suggest that ours is perhaps the first example of such a phenomenon in three dimensions and where the QSL state is reached through an intermediate VBS state.

Experimental results—$Y_3Cu_2Sb_3O_{14}$ crystallizes in the $R\bar{3}m$ space group at room temperature where Cu^{2+} triangular layers are stacked by alternating Y and Sb kagome layers. Its crystal structure is illustrated in Fig. 1(a). There are two different crystallographic sites for Cu atoms, corresponding to Cu(1) at the $3a$ or (0, 0, 0) and to Cu(2) at the $3b$ or (0, 0, 1/2) positions [see Ref. [22] for details]. There is a threefold rotation symmetry around the c-axis at both the sites, as dictated by the crystal symmetry [see Figs. 1(b) and 1(c)].

The ^{89}Y NMR line splits below about 120 K (see Ref. [22] for details) and the fractional line shift of the component, which continues to increase at lower T and varies in a Curie-Weiss (CW) manner with an antiferromagnetic (AF) $\theta_{CW} = -23(1)$ K [open symbols in Fig. 2(a)]. The other component [solid symbols in Fig. 2(a)] has a shift $^{89}K(T)$, which drops sharply at about 120 K and remains small at lower temperatures, consistent with condensation into a singlet state. Further, we have measured the ^{89}Y NMR spin-lattice relaxation rate T_1^{-1} [see Fig. 2(b)] at each of the peaks to investigate the low-energy

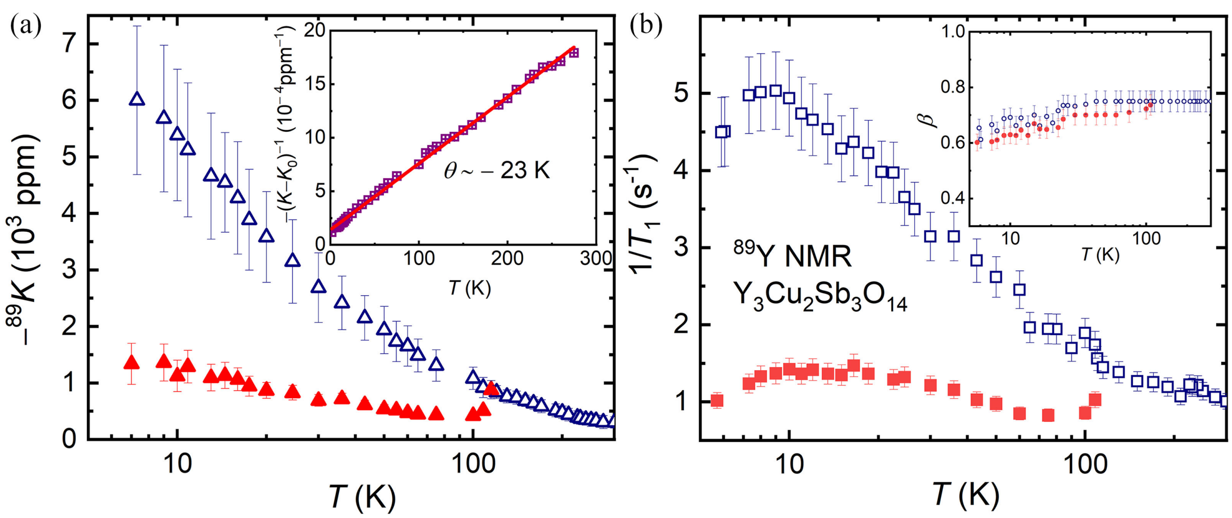

FIG. 2. (a) Variation of NMR shift, ^{89}K with temperature. Inset: $(K\text{-}K_0)^{-1}$ vs T and solid red line represent Curie-Weiss fitting. Here, K is the NMR shift of the more shifted line (open triangles in the main figure). (b) Spin-lattice relaxation rate ($1/T_1$) as a function of temperature. The inset shows the stretching exponent β as a function of temperature.

spin dynamics in $Y_3Cu_2Sb_3O_{14}$. The nuclear magnetization recovery is well fitted with a stretched exponential $\{M(t) = M_0[1 - Ae^{-(t/T_1)^\beta}]\}$. At high temperature, T_1^{-1} gradually increases as the temperature decreases. A sharp change is observed around 120 K, below which T_1^{-1} is different at the two peak positions. T_1^{-1} corresponding to the more shifted peak continues to increase with decreasing temperature (together with a Curie-like increase of its shift, K) and finally decreases below 10 K. The T_1^{-1} corresponding to the less shifted peak falls sharply (consistent with a line position that is nearly at the diamagnetic reference position) below 120 K, then increases slightly and exhibits a plateau from 20 K to 10 K, and drops thereafter. A broad maximum in T_1^{-1} has been observed in numerous organic spin liquid candidates [40–42], where it is attributed to the relaxation of impurity spins, and this might be the case here as well. The decrease of the effective moment below about 120 K is demonstrated by having a fraction of the spins dropping out from the CW behavior and becoming a part of the VBS phase. It is reasonable to say that the slower component arises from the fraction that has condensed into a VBS state, while the faster component is from the fraction that remains paramagnetic below 120 K but eventually also condenses into a QSL state below about 10 K. In Lab-based XRD, we did not observe any change in the structure around 120 K as one might expect from a symmetry breaking. However, it is possible that there is only a subtle structural change (a small change in bond lengths and bond angles) associated with the symmetry breaking VBS transition. This partial VBS formation could also be due to chemical disorder. This scenario is akin to that in $LiZn_2Mo_3O_8$, where the triangular lattice decouples into a honeycomb lattice (which condenses into a VBS state) plus free spins at the center of the honeycombs [4–6]. In the present case, given the three-dimensional geometry, it is not obvious what the decoupled lattice might be, though it is primarily thought to be made of body-diagonals of the distorted cubes in the structure [see Fig. 1(b)].

We next examine the low-energy excitations and spin dynamics through specific heat and muon spin relaxation (μSR) measurements. The magnetic specific heat $C_{mag}(T)$ (see Fig. 3) was obtained by subtracting the lattice contribution obtained from the data of the nonmagnetic structural analog $Lu_3Zn_2Sb_3O_{14}$ (see Ref. [22] for details). $C_{mag}(T)$ exhibits a broad hump at 10 K followed by a plateau around 1 K. The low-T plateau is suppressed in fields greater than 30 kOe. The entropy change calculated by integrating the $C_{mag}(T)/T$ vs T data is shown in Fig. 3 (inset). Close to 40% of the entropy (compared to $R\ln 2$) is recovered by about 20 K. In our suggested scenario, a fraction of the spins condense into a VBS below about 120 K, while all the spins condense to a gapless QSL state below about 10 K. So, a part of the entropy release would happen at about 120 K, while the remaining would be around 10 K. We observe the lower temperature plateau

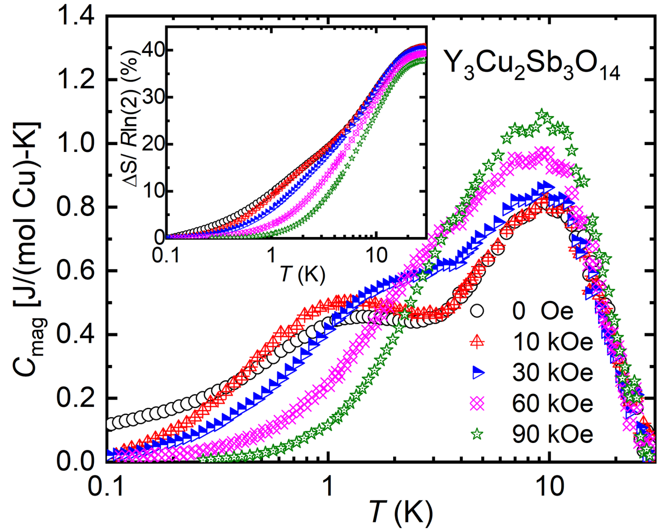

FIG. 3. The temperature dependence of the magnetic specific heat in several magnetic fields. The inset depicts the temperature dependence of associated magnetic entropy change ΔS, normalized to $R\ln(2)$ per mol Cu.

around 20 K, while the higher temperature plateau is difficult to obtain reliably due to the uncertainty in inferring the magnetic contribution by subtracting the lattice contribution, which is large and dominant already beyond 20 K.

We next detail our μSR data and analysis, which show signatures of two plateaus with decreasing temperature. The time-dependent zero-field (ZF) asymmetry spectra for $Y_3Cu_2Sb_3O_{14}$ displayed in Fig. 4 confirm the absence of any coherent oscillations or any initial asymmetry drop in the spectra down to 0.077 K. Furthermore, there is no indication of a 1/3 recovery of the muon polarization at long times, which precludes the occurrence of any long-range static magnetic order. The ZF μSR spectra are well fitted by a Gaussian Kubo-Toyabe (KT) function, G_{ZF}^{KT}, multiplied by an exponential function, and a temperature-independent background, P_{BG}, arising from the silver sample holder or the cryostat:

$$P(t) = P_0 \exp(-\lambda_{ZF} t) G_{ZF}^{KT}(\Delta, t) + P_{BG}, \tag{1}$$

where P_0 is the initial asymmetry and λ_{ZF} represents the ZF relaxation rate caused by the electronic Cu spins (see Ref. [22] for details).

The obtained λ_{ZF} is plotted against temperature in Fig. 4 (inset). With decreasing temperature, λ_{ZF} increases, and then, holds a plateau in the temperature range 65 K $\gtrsim T \gtrsim$ 10 K. With further cooling below 10 K, λ_{ZF} increases gradually, and then, saturates at about $T \approx 1$ K and remains constant down to the lowest measured temperature, 0.077 K. Our longitudinal field data (see Ref. [22] for details) show that the muon spin is not decoupled from the internal moments, even in fields of 3200 Oe. This result

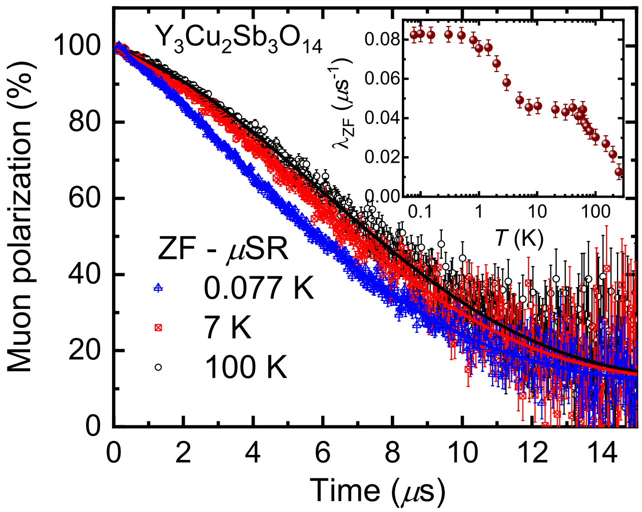

FIG. 4. The time evolution of the ZF-μSR asymmetry spectra at selected temperatures, where solid lines are the fits to Eq. (1). Inset shows the temperature dependence of the muon spin relaxation rate, λ_{ZF}, extracted from fits to the data.

shows that $Y_3Cu_2Sb_3O_{14}$ enters a low-T regime where the spin dynamics are persistent and temperature independent. Such behavior has been observed in numerous other proposed QSL candidates [23,43]. Finally, the bulk magnetic susceptibility $\chi(T)$ (see Ref. [22] for details) varies in a Curie-Weiss manner (high-temperature Curie-Weiss temperature $\theta_{CW} \simeq -23(1)$ K and an effective moment $\mu_{eff} = 1.57\mu_B$), with the absence of any anomalies suggesting the absence of any long-range order down to 0.40 K. Furthermore, no apparent difference is seen between the zero field cooled and field cooled susceptibility $\chi(T)$ data taken in an applied magnetic field $H \approx 100$ Oe, which excludes the occurrence of spin freezing. Also, from a plot of the inverse susceptibility with temperature (see Ref. [22] for details), we find a change of slope around 60 K, below which the Curie term shows a small decrease. The ESR data allow us to identify the fraction of copper spins forming dimers below 120 K as about 20% of all copper spins. Its intensity can be well described by the characteristic Bleaney-Bowers law for the magnetic susceptibility of spin dimers see Ref. [22] for details. The remaining 80% are ESR silent, probably due to strong spin-phonon interaction, like in the high-T_c cuprates. Only a small fraction of these unpaired spins shows up in the ESR spectra at low temperature, revealing a very large linewidth, which strongly increases with increasing temperature, so that the signal becomes undetectable above 25 K. This supports the assumption of randomly distributed antiferromagnetic couplings between the residual spins after dimerization of the 20% fraction.

Electronic structure calculation—To check the viability of a quantum spin liquid, we carried out first principles electronic structure calculations based on density functional theory (DFT) for the experimentally determined rhombohedral pyrochlore structure of $Y_3Cu_2Sb_3O_{14}$. All the electronic structure calculations were carried out using DFT in the pseudopotential plane-wave basis within the generalized gradient approximation [44] supplemented with Hubbard U [45] as encoded in the Vienna *ab initio* simulation package [46,47] with projector augmented wave potentials [48,49]. The calculations were done with standard values of $U_{eff} \equiv U_d - J_H = 6.5$ eV [45] chosen for Cu. The non-spin-polarized total, Cu-d and O-p partial density of states for $Y_3Cu_2Sb_3O_{14}$ (see Ref. [22] for details), reveal that the Fermi level is dominated by half-filled Cu(1) e_g and Cu(2) a_{1g} states, and the O-p states are fully occupied, while the Sb-s, Sb-p, Y-s, and Y-d states are completely empty, consistent with the nominal ionic formula of this compound, $Y_3{}^{3+}Cu_2{}^{2+}Sb_3{}^{5+}O_{14}{}^{2-}$ (see Ref. [22] for details). Spin-polarized calculations with ferromagnetic arrangement of Cu spins yields a total moment of 2.0 μ_B per formula unit, which further supports the $S = \frac{1}{2}$ moment of the Cu atom and is consistent with the experimentally determined effective moment ($\mu_{eff} = 1.57\mu_B$). However, the calculated magnetic moment per Cu site is 0.80 μ_B [0.80 μ_B for Cu(1) and 0.76 μ_B for Cu(2)], where the rest of the moment is shared with the ligand atoms due to substantial hybridization of the Cu atoms with ligands.

The crystal structure is such that the nearest-neighbor arrangement between Cu(1) and Cu(2) forms a slightly distorted cubic structure with unequal body diagonals, as shown in Fig. 5, where each Cu(2) is a nearest neighbor to a Cu(1). The exchange path between two inequivalent Cu atoms forming the body diagonal is shown in Fig. 5(a) with violet shades. In addition, we have shown the exchange path along the face diagonals either between Cu(1) and Cu(1) or Cu(2) and Cu(2) in Fig. 5(b), forming a triangular network.

We have calculated these exchange interactions by employing the "four state" method [50–52]. This is based

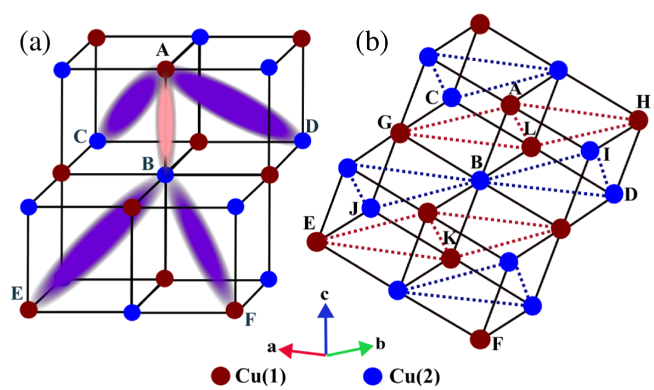

FIG. 5. (a) A schematic of the slightly distorted cubic structure formed by the nearest-neighbor Cu-Cu network in $Y_3Cu_2Sb_3O_{14}$. The brown dots represent Cu(1) atoms, and blue dots represent Cu(2) atoms. The different exchange paths are also shown. (b) The different in-plane triangular networks formed by the Cu atoms are shown by the dotted lines.

TABLE I. Exchange parameters along the body diagonals.

J	Cu-Cu distance (Å)	Exchange parameter (meV)
J_{AC}	9.01	3.6
J_{AD}	9.01	4.6
J_{BE}	9.01	3.6
J_{BF}	8.58	3.0
J_{AB}	5.14	0.2

on a computation of the total energy of the system with collinear spin alignment, where the spin configurations on the two chosen sites are modified while restricting the rest of the spins to a ferromagnetic configuration. The calculated exchange parameters along body diagonals are presented in Table I. The exchange parameters along the face diagonal, where each of the Cu(1) and Cu(2) ions form a triangular network, are shown in Table II. Calculations reveal that the dominant exchange interactions are along the body diagonals of the cube, forming dimers where the interdimer exchange interaction (J_{AB}) is negligible compared to the intradimer exchange interactions. The difference between the intradimer and interdimer interactions may be attributed to the geometry of the super-super exchange path mediated by oxygens, which is nearly linear for the intradimer exchange and substantially distorted for the interdimer exchange path. As a consequence, in spite of the short interdimer distance, the intradimer exchange interaction dominates [53]. This opens up the possibility for the formation of VBS within our system. The antiferromagnetic interaction along the face diagonal of the cube forming a triangular network for Cu(1) and Cu(2) introduces frustration and prohibits long-range ordering. Our first principles DFT results corroborate well with the experimental results and lend credence to the scenario of spin liquid behavior in this three-dimensional system induced by frustration.

Conclusion—Our comprehensive measurements on $Y_3Cu_2Sb_3O_{14}$ have established that in spite of a sizable exchange interaction corresponding to an AF $\theta_{CW} = -23$ K, the compound does not order down to 0.077 K. More importantly, unlike other candidate QSLs, the present compound shows *two* crossovers with decreasing temperature. The signatures of the higher temperature condensation (bifurcation at 120 K in NMR, a plateau below about 60 K in μSR λ_{ZF}, and a dimer fit of the ESR intensity) are apparent in our data, while those of the low-T one are distinctly seen in our μSR and ESR data, though hints are also present in NMR and specific heat.

Backed by the evidence we have presented, we suggest that the higher temperature plateau corresponds to the condensation of a fraction of the spins into a VBS state, while all the spins condense into a QSL state below 1 K. This novel result in a three-dimensional frustrated magnet should spark intense activity to examine magnetic excitations through neutron scattering in this compound.

TABLE II. Exchange parameters along the face diagonals or in the Cu(1) planes and Cu(2) planes.

J	Cu-Cu distance (Å)	Exchange parameter (meV)
J_{AH}	7.40	2.2
J_{AL}	7.40	1.6
J_{HL}	7.40	1.5
J_{BI}	7.40	2.0
J_{ID}	7.40	2.1
J_{BD}	7.40	1.7

Acknowledgments—We thank DST-SERB for funding under the DST-CRG scheme (CRG/2021/003024). We acknowledge the use of various central facilities at IIT Bombay. Experiments at the ISIS Neutron and Muon Source were supported by a beam-time allocation RB2410186 [54] from the Science and Technology Facilities Council UK (funded via the ISIS-Indian Partnership agreement). We acknowledge UGC-DAE CSR (Indore) for providing the mK specific heat experimental facility (01/2024/6185). S. N. would like to acknowledge funding support for the Chanakya postdoctoral fellowship (CPDF/2021-22/01) from the National Mission on Interdisciplinary Cyber Physical Systems, of the DST, Govt. of India through the I-HUB Quantum Technology Foundation. This work was partially supported by the Deutsche Forschungsgemeinschaft (DFG) within the Transregional Collaborative Research Center TRR 360 "Constrained Quantum Matter", Project No. 492547816 (Augsburg, Munich, Stuttgart, Leipzig). We thank Dr. Rahul Kumar and Dr. A. Sundaresan (Jawaharlal Nehru Centre for Advanced Scientific Research) for their support with dc magnetization measurements using a ^{3}He attachment to the MPMS. I. D. and R. D. would like to thank Dr. Atasi Chakraborty for discussions.

Data availability—The data that support the findings of this article are not publicly available. The data are available from the authors upon reasonable request.

[1] T.-H. Han, J. S. Helton, S. Chu, D. G. Nocera, J. A. Rodriguez-Rivera, C. Broholm, and Y. S. Lee, Fractionalized excitations in the spin-liquid state of a kagome-lattice antiferromagnet, Nature (London) **492**, 406 (2012).

[2] Y. Okamoto, H. Yoshida, and Z. Hiroi, Vesignieite $BaCu_3V_2O_8(OH)_2$ as a candidate spin-1/2 kagome antiferromagnet, J. Phys. Soc. Jpn. **78**, 033701 (2009).

[3] Y. Zhou, K. Kanoda, and T.-K. Ng, Quantum spin liquid states, Rev. Mod. Phys. **89**, 025003 (2017).

[4] J. P. Sheckelton, J. R. Neilson, D. G. Soltan, and T. M. McQueen, Possible valence-bond condensation in the frustrated cluster magnet $LiZn_2Mo_3O_8$, Nat. Mater. **11**, 493 (2012).

[5] R. Flint and P. A. Lee, Emergent honeycomb lattice in $LiZn_2Mo_3O_8$, Phys. Rev. Lett. **111**, 217201 (2013).
[6] J. P. Sheckelton, F. R. Foronda, L. D. Pan, C. Moir, R. D. McDonald, T. Lancaster, P. J. Baker, N. P. Armitage, T. Imai, S. J. Blundell, and T. M. McQueen, Local magnetism and spin correlations in the geometrically frustrated cluster magnet $LiZn_2Mo_3O_8$, Phys. Rev. B **89**, 064407 (2014).
[7] S. Chillal, Y. Iqbal, H. O. Jeschke, J. A. Rodriguez-Rivera, R. Bewley, P. Manuel, D. Khalyavin, P. Steffens, R. Thomale, A. N. Islam, and B. Lake, Evidence for a three-dimensional quantum spin liquid in $PbCuTe_2O_6$, Nat. Commun. **11**, 2348 (2020).
[8] Z. L. Dun, J. Trinh, K. Li, M. Lee, K. W. Chen, R. Baumbach, Y. F. Hu, Y. X. Wang, E. S. Choi, B. S. Shastry, A. P. Ramirez, and H. D. Zhou, Magnetic ground states of the rare-earth tripod kagome lattice $Mg_2RE_3Sb_3O_{14}$ (RE = Gd, Dy, Er), Phys. Rev. Lett. **116**, 157201 (2016).
[9] Z. L. Dun, J. Trinh, M. Lee, E. S. Choi, K. Li, Y. F. Hu, Y. X. Wang, N. Blanc, A. P. Ramirez, and H. D. Zhou, Structural and magnetic properties of two branches of the tripod-kagome-lattice family $A_2R_3Sb_3O_{14}$ (A = Mg, Zn; R = Pr, Nd, Gd, Tb, Dy, Ho, Er, Yb), Phys. Rev. B **95**, 104439 (2017).
[10] J. A. Paddison, H. S. Ong, J. O. Hamp, P. Mukherjee, X. Bai, M. G. Tucker, N. P. Butch, C. Castelnovo, M. Mourigal, and S. Dutton, Emergent order in the kagome ising magnet $Dy_3Mg_2Sb_3O_{14}$, Nat. Commun. **7**, 13842 (2016).
[11] W. Fu and D. IJdo, Crystal structure of $Mn_2Ln_3Sb_3O_{14}$ (Ln = La, Pr and Nd): a new ordered rhombohedral pyrochlore, J. Solid State Chem. **213**, 165 (2014).
[12] V. Kumar, S. Kundu, M. Baenitz, and A. Mahajan, Magnetic transition in the $J_{\mathrm{eff}} = 1/2$ kagomé system $Sm_3Sb_3Zn_2O_{14}$, J. Magn. Magn. Mater. **552**, 169145 (2022).
[13] C. Lee, S. Lee, H.-S. Kim, S. Kittaka, Y. Kohama, T. Sakakibara, K. H. Lee, J. van Tol, D. I. Gorbunov, S.-H. Do, S. Yoon, A. Berlie, and K.-Y. Choi, Random singlets in the $S = 5/2$ coupled frustrated cubic lattice $Lu_3Sb_3Mn_2O_{14}$, Phys. Rev. B **107**, 214404 (2023).
[14] C. Lee, S.-K. Lee, S. Lee, J. van Tol, and K.-Y. Choi, Random-singlet-like state emergent in $S = 5/2$ frustrated cubic lattice, J. Korean Phys. Soc. **84**, 151 (2024).
[15] Y. Yang, X. Li, C. Tan, Z. Zhu, J. Zhang, Z. Ding, Q. Wu, C. Chen, T. Shiroka, Y. Xia *et al.*, Intrinsic new properties of a quantum spin liquid, arXiv:2102.09271.
[16] O. Bradley, Y. Zhang, J. Oitmaa, and R. R. Singh, High-temperature magnetization and entropy of the triangular lattice hubbard model in a zeeman field, arXiv:2303.03550.
[17] K. Li, Y. Hu, Y. Wang, T. Kamiyama, B. Wang, Z. Li, and J. Lin, Syntheses and properties of a family of new compounds $RE_3Sb_3Co_2O_{14}$ (RE = La, Pr, Nd, Sm–Ho) with an ordered pyrochlore structure, J. Solid State Chem. **217**, 80 (2014).
[18] S. Mayouf, C. Vincent, M. Fadia, Z. Kheira, T. Bouazza, and B. Naceur, Synthesis and characterization of a new ordered rhombohedral pyrochlore family $Ln_3Sb_3Cu_2O_{14}$ (Ln = Pr, Nd, Sm, Eu, Tb, Dy) with more detailed study of the Sm compound, J. Solid State Chem. **326**, 124205 (2023).
[19] M. B. Sanders, K. M. Baroudi, J. W. Krizan, O. A. Mukadam, and R. J. Cava, Synthesis, crystal structure, and magnetic properties of novel 2D kagome materials $RE_3Sb_3Mg_2O_{14}$ (RE = La, Pr, Sm, Eu, Tb, Ho): Comparison to $RE_3Sb_3Zn_2O_{14}$ family, Phys. Status Solidi B **253**, 2056 (2016).
[20] M. B. Sanders, J. W. Krizan, and R. J. Cava, $RE_3Sb_3Zn_2O_{14}$ (RE = La, Pr, Nd, Sm, Eu, Gd): A new family of pyrochlore derivatives with rare earth ions on a 2D kagome lattice, J. Mater. Chem. C **4**, 541 (2016).
[21] A. Scheie, M. Sanders, J. Krizan, Y. Qiu, R. J. Cava, and C. Broholm, Effective spin-1/2 scalar chiral order on kagome lattices in $Nd_3Sb_3Mg_2O_{14}$, Phys. Rev. B **93**, 180407(R) (2016).
[22] See Supplemental Material at http://link.aps.org/supplemental/10.1103/2bps-xvl8 for the supporting results and discussion, which includes Refs. [11,13,23–39].
[23] Y. S. Choi, C. H. Lee, S. Lee, S. Yoon, W.-J. Lee, J. Park, A. Ali, Y. Singh, J.-C. Orain, G. Kim, J.-S. Rhyee, W.-T. Chen, F. Chou, and K.-Y. Choi, Exotic low-energy excitations emergent in the random kitaev magnet Cu_2IrO_3, Phys. Rev. Lett. **122**, 167202 (2019).
[24] J. Rodríguez-Carvajal, Recent advances in magnetic structure determination by neutron powder diffraction, Physica (Amsterdam) **192B**, 55 (1993).
[25] G. A. Bain and J. F. Berry, Diamagnetic corrections and Pascal's constants, J. Chem. Educ. **85**, 532 (2008).
[26] K. Kitagawa, T. Takayama, Y. Matsumoto, A. Kato, R. Takano, Y. Kishimoto, S. Bette, R. Dinnebier, G. Jackeli, and H. Takagi, A spin–orbital-entangled quantum liquid on a honeycomb lattice, Nature (London) **554**, 341 (2018).
[27] F. Bahrami, W. Lafargue-Dit-Hauret, O. I. Lebedev, R. Movshovich, H.-Y. Yang, D. Broido, X. Rocquefelte, and F. Tafti, Thermodynamic evidence of proximity to a kitaev spin liquid in $Ag_3LiIr_2O_6$, Phys. Rev. Lett. **123**, 237203 (2019).
[28] E. M. Kenney, C. U. Segre, W. Lafargue-Dit-Hauret, O. I. Lebedev, M. Abramchuk, A. Berlie, S. P. Cottrell, G. Simutis, F. Bahrami, N. E. Mordvinova, G. Fabbris, J. L. McChesney, D. Haskel, X. Rocquefelte, M. J. Graf, and F. Tafti, Coexistence of static and dynamic magnetism in the kitaev spin liquid material Cu_2IrO_3, Phys. Rev. B **100**, 094418 (2019).
[29] I. Kimchi, A. Nahum, and T. Senthil, Valence bonds in random quantum magnets: Theory and application to $YbMgGaO_4$, Phys. Rev. X **8**, 031028 (2018).
[30] M. Bouvier, P. Lethuillier, and D. Schmitt, Specific heat in some gadolinium compounds. I. experimental, Phys. Rev. B **43**, 13137 (1991).
[31] I. Kimchi, J. P. Sheckelton, T. M. McQueen, and P. A. Lee, Scaling and data collapse from local moments in frustrated disordered quantum spin systems, Nat. Commun. **9**, 4367 (2018).
[32] M. Pula, S. Sharma, J. Gautreau, K. P. S., A. Kanigel, M. D. Frontzek, T. N. Dolling, L. Clark, S. Dunsiger, A. Ghara, and G. M. Luke, Candidate for a quantum spin liquid ground state in the shastry-sutherland lattice material $Yb_2Be_2GeO_7$, Phys. Rev. B **110**, 014412 (2024).
[33] K. Bhattacharya, S. Mohanty, A. D. Hillier, M. T. F. Telling, R. Nath, and M. Majumder, Evidence of quantum spin liquid state in a Cu^{2+}-based $S = 1/2$ triangular lattice antiferromagnet, Phys. Rev. B **110**, L060403 (2024).

[34] F. Pratt, WIMDA: a muon data analysis program for the Windows PC, Physica (Amsterdam) **289B**, 710 (2000).

[35] S. Nandi, Y. Jana, D. Swarnakar, J. Alam, P. Bag, and R. Nath, Magnetization process and specific heat properties of geometrically frustrated pyrochlores R_2FeSbO_7 ($R^{3+} = Dy$, Y) and spin-ice magnetic phase in Dy_2FeSbO_7, J. Alloys Compd. **714**, 318 (2017).

[36] A. Abragam and B. Bleaney, *Electron Paramagnetic Resonance of Transition Ions* (Oxford University Press, Oxford, 2012).

[37] N. Zhuk, S. Nekipelov, V. Sivkov, N. Sekushin, V. Lutoev, B. Makeev, A. Koroleva, A. Fedorova, L. Koksharova, M. Ignatova *et al.*, Magnetic and electric properties, ESR, XPS and NEXAFS spectroscopy of $CaCu_3Ti_4O_{12}$ ceramics, Ceram. Int. **46**, 21410 (2020).

[38] B. Kochelaev, Spin-phonon interaction and the EPR line-width in La_2CuO_4 and related cuprates, J. Supercond. **12**, 53 (1999).

[39] B. Bleaney and K. Bowers, Anomalous paramagnetism of copper acetate, Proc. R. Soc. A **214**, 451 (1952).

[40] A. Pustogow, T. Le, H.-H. Wang, Y. Luo, E. Gati, H. Schubert, M. Lang, and S. E. Brown, Impurity moments conceal low-energy relaxation of quantum spin liquids, Phys. Rev. B **101**, 140401(R) (2020).

[41] A. Pustogow, Thirty-year anniversary of κ-$(BEDT\text{-}TTF)_2Cu_2(CN)_3$: Reconciling the spin gap in a spin-liquid candidate, Solids **3**, 93 (2022).

[42] T. Itou and R. Kato, ^{13}C NMR reexamination of the valence bond solid state in $EtMe_3P[Pd(dmit)_2]_2$, Phys. Rev. B **108**, 104410 (2023).

[43] S. Kundu, A. Shahee, A. Chakraborty, K. M. Ranjith, B. Koo, J. Sichelschmidt, Mark T. F. Telling, P. K. Biswas, M. Baenitz, I. Dasgupta, S. Pujari, and A. V. Mahajan, Gapless quantum spin liquid in the triangular system $Sr_3CuSb_2O_9$, Phys. Rev. Lett. **125**, 267202 (2020).

[44] J. P. Perdew, K. Burke, and M. Ernzerhof, Generalized gradient approximation made simple, Phys. Rev. Lett. **77**, 3865 (1996).

[45] V. I. Anisimov, J. Zaanen, and O. K. Andersen, Band theory and Mott insulators: Hubbard U instead of Stoner I, Phys. Rev. B **44**, 943 (1991).

[46] G. Kresse and J. Hafner, *Ab initio* molecular dynamics for liquid metals, Phys. Rev. B **47**, 558 (1993).

[47] G. Kresse and J. Furthmüller, Efficient iterative schemes for *ab initio* total-energy calculations using a plane-wave basis set, Phys. Rev. B **54**, 11169 (1996).

[48] P. E. Blöchl, Projector augmented-wave method, Phys. Rev. B **50**, 17953 (1994).

[49] G. Kresse and D. Joubert, From ultrasoft pseudopotentials to the projector augmented-wave method, Phys. Rev. B **59**, 1758 (1999).

[50] H. J. Xiang, E. J. Kan, S.-H. Wei, M.-H. Whangbo, and X. G. Gong, Predicting the spin-lattice order of frustrated systems from first principles, Phys. Rev. B **84**, 224429 (2011).

[51] R. Kumar, T. Dey, P. M. Ette, K. Ramesha, A. Chakraborty, I. Dasgupta, R. Eremina, S. Tóth, A. Shahee, S. Kundu, M. Prinz-Zwick, A. A. Gippius, H. A. Krug von Nidda, N. Büttgen, P. Gegenwart, and A. V. Mahajan, Structural, thermodynamic, and local probe investigations of the honeycomb material $Ag_3LiMn_2O_6$, Phys. Rev. B **99**, 144429 (2019).

[52] X. Li, H. Yu, F. Lou, J. Feng, M.-H. Whangbo, and H. Xiang, Spin hamiltonians in magnets: Theories and computations, Molecules **26**, 803 (2021).

[53] H. C. Walker, O. Mustonen, S. Vasala, D. J. Voneshen, M. D. Le, D. T. Adroja, and M. Karppinen, Spin wave excitations in the tetragonal double perovskite Sr_2CuWO_6, Phys. Rev. B **94**, 064411 (2016).

[54] S. Nandi *et al.*, Possible quantum spin liquid phase in the $S = 1/2$ frustrated cubic lattice $Y_3Cu_2Sb_3O_{14}$, STFC ISIS Neutron and Muon Source (2024), 10.5286/ISIS.E.RB 2410186.